Identification and Functional Characterization of Long Non-coding RNA *MIR22HG* as a Tumor Suppressor for Hepatocellular Carcinoma

Dong-Yan Zhang[1, 2 †], Xue-Jing Zou[2, 3†], Chuan-Hui Cao[1, 2], Ting Zhang[2, 4], Ling Lei[1, 2], Xiao-Long Qi, Li Liu[2, 3, 4*] and De-Hua Wu[1, 2*]

Supplementary materials and methods

qRT-PCR

TRIzol® reagent (Invitrogen, Carlsbad, CA, USA) was used for the extraction of total RNAs. First-strand cDNA was synthesized by the PrimeScript™ 1st Strand cDNA Synthesis Kit (TaKaRa, Tokyo, Japan). Real-time PCR was carried out using SYBR® Green PCR kit (TaKaRa). Primers were shown in Supplementary Table 5.

Plasmid construction and transient transfection

Wild type HMGB1 3'-UTR sequence (containing miR-22-3p binding site) and mutant HMGB1 3'-UTR sequence (miR-22-3p binding site mutation) were amplified and inserted into psiCHECKTM-2 Vector (Promega, Madison, WI, USA) to construct plasmids used in the following dual-luciferase reporter assays. The open reading frame (ORF) of HMGB1 was cloned and inserted into pCMV6-AC-GFP (Origene, Rockville, MD, USA) vector to generate HMGB1. The primer sequences were listed in Supplementary Table 5. Cells seeded overnight were transiently transfected with

plasmids or control vectors at 90% cell confluency using Lipofectamine 2000 (Invitrogen). 48 hours later, cells were harvested for following assays.

Lentiviral construction and transduction

The lentiviral vector containing full-length of human *MIR22HG* gene sequence was achieved from Genechem Company Ltd (Shanghai, China). Lentiviral vector containing full-length of human *MIR22HG* gene sequence or the empty lentiviral vector were introduced to SK-Hep-1 and SMMC-7721 cells according to the manufacture's instruction. To select clones stably overexpressing *MIR22HG*, cells after transfection were exposed to puromycin for 2 weeks. 2 weeks later, cells were harvested for RNA isolation. The expression of *MIR22HG* was then determined using qRT-PCR.

Cell counting kit-8 (CCK-8) assays

Cellular proliferation capacity was tested with Cell Counting Kit 8 (CCK-8) assay (Dojindo, Kumamoto, Japan) following the manufacturer's protocol. 1×10^3 cells per well were seeded in 96-well plate and grow for the given time points. 24 hours later, 10μl CCK-8 reagent was added to each plate, and cultured for another 2 hours at 37 °C. Then optical density was test at 450nm. All experiments were performed in triplicate.

5-ethynyl-20-deoxyuridine (EdU) incorporation assays

SMMC-7721 cells seeded in 24-well plates were cultured in humidified incubator for 12h. Cells were transiently transfected with vectors or siRNAs 12h later according to the protocol. EdU Cell Proliferation Assay Kit (Ribobio, Wuhan, China) were used to detect the cellular proliferation after 48h. Briefly, fixed SMMC-7721 cells were stained with EdU following the recommendations after incubation with 50μM EdU. The ratio of EdU positive cells to total Hoechst positive cells was regarded as EdU incorporation rate.

miRNA transfection

The miR-22-3p mimic and miR-22-3p inhibitor were obtained from Shanghai Genepharma Company, China. The miRNA mimics or inhibitor were introduced into HCC cells using Lipofectamine RNAiMAX Transfection Reagent (Invitrogen) following the manufacturer's instruction. After incubation for 24-48 hours, cells were ready for the following assays.

Luciferase reporter assays

SMMC-7721 cells were cultured in 24-well plates and co-transfected with 40ng plasmids containing wild type HMGB1 3'-UTR sequences (termed psiCHECK-wt-HMGB1) or plasmids containing mutant HMGB1 3'-UTR sequences (termed psiCHECK-mut-HMGB1) and 20 pmol miR-22-3p mimic or negative control. Luciferase activities of both firefly and Renilla were examined using the Dual-Luciferase® Reporter Assay System ((Promega) 48 hours later.

RNA interference

Small interfering RNAs were used in the current study to silence human *MIR22HG* gene expression. All target sequences for *MIR22HG* were synthesized by Genepharma Company and listed in Supplementary Table 6. Lipofectamine RNAiMAX Transfection Reagent (Invitrogen) was used to perform transfection assays.

***In situ* hybridization (ISH)**

ISH was carried out with the ISH Kit (Boster Bio-Engineering Company, Wuhan, China) to explore the expression of *MIR22HG* in HCC tissue and matched non-tumor tissues. Two pathologists who blinded to the clinical parameters reviewed and scored the ISH-staining regions for *MIR22HG*. The staining intensity was scored as follows: 0 (negative), 1 (weak), 2 (medium), 3 (strong). The score of staining extent was as follows: 0 (10%), 1 (1%-25%), 2 (26%-50%), 3 (51%-75%), and 4(76%-100%). The total score for *MIR22HG* was calculated based on the intensity and extent scores, ranging from 0 to 7. A total score ≥4 was defined as belonging in the high-expression group.

Immunohistochemistry (IHC)

IHC staining was performed to determine the expression of Ki-67 and HMGB1 in tumor tissues from subcutaneous xenograft model using Dako Envision System (Dako, Carpinteria, CA, USA) according to the manufacturer's recommended protocol. The

tumor tissues were fixed with 10% formalin, embedded in paraffin, and then sectioned 4 μm in thickness. After baking at 65°C for 2 hours, sections were deparaffinized and rehydrated. Sections were submerged in sodium citrate buffer (pH 6.0) for antigen retrieval. After incubation with 0.3% H_2O_2 for 15 min to block the endogenous peroxidase, the sections were incubated with antibody for Ki-67 or HMGB1 overnight at 4°C. Sections were incubated with peroxidase labeled polymer conjugated to a secondary antibody at room temperature for 50 minutes after washing. Finally, diaminobenzidine (DAB) was used for color reactions.

Western blot

Total protein was extracted using RIPA buffer (Cell signaling Technology, Boston, MA, USA). The protein lysates were separated on a 12% SDS–polyacrylamide gel, and transferred onto polyvinylidene fluoride (Millipore, Bedford, MA, USA) membranes. After blocking with 5% BSA for 1 hour at room temperature, the membranes were incubated with primary antibodies overnight at 4°C. After washing, the membranes were incubated with the corresponding secondary antibodies conjugated to horseradish peroxidase. The membrane signals were detected using commercial ECL kit (Pierce, Rockford, IL, USA). Image J program was used to analyze the band intensity of western blotting and the normalization. The primary antibodies were shown in Supplementary Table 7.

RNA-Binding Protein Immunoprecipitation (RIP) analyses

RIP assay was carried out following recommendations of the Magna RIP RNA-Binding Protein Immunoprecipatation Kit (Millipore, Bedford, MA). In brief, magnetic beads were pre-incubated with an anti-HuR antibody or anti-mouse IgG for about 30 minutes at room temperature. 30 minutes later, magnetic beads were washed with RIP wash buffer. After washing, cell lysates were immunoprecipitated with magnetic beads at 4^{o}C overnight. After immunoprecipitation, magnetic beads were washed with RIP wash buffer for 5 times. RNA which bound to beads was then purified from RNA-protein complexes, and analyzed using qRT-PCR.

RNA Pull-Down Assays

RNAs were *in vitro* transcribed using T7 RNA polymerase (Thermo scientific Transcript Aid T7 High Yield Transcription Kit, Waltham, MA) and biotin-labeled using Pirece^{TM} RNA 3' End Desthiobiotiny Kit (Thermo Fisher scientific). RNA pull-down assay was performed following the instructions of the Pierce^{TM} Magnetic RNA-Protein Pull-Down Kit (Thermo Fisher scientific). Magnetic Beads were subjected to RNA (50 pmol) capture in RNA capture buffer (20mM Tris-HCl pH 7.5, 1M NaCl, 1mM EDTA) for 15-30 min at room temperature under agitation. The RNA-captured beads were washed once with 50µl 20mM Tris (pH 7.5) and incubated with 2 mg SMMC-7721 cell lysates for 30-60 min at 4°C under rotation. The RNA-binding protein complexes were then washed twice with wash buffer (20mM Tris-HCl pH 7.5, 10mM NaCl, 0.1% Tween-20 Detergent) and eluted with Biotin Elution Buffer.

Immunofluorescence assay

SMMC-7721 cells transfected with *MIR22HG* and *MIR22HG*-mut were seeded on coverslips. 24h later, cells on coverslips were washed with phosphate-buffered saline (PBS), fixed with 4% paraformaldehyde for 15 minutes, and then permeabilized with 0.25% Triton for 10 minutes. After that, cells were incubated with anti-HuR antibody at 4^{o}C overnight. Cells were incubated with rhodamineconjugated goat antibodies against mouse IgG (Abcam, Cambridge, UK) after washing with PBS for 5 times. Nuclei was stained with DAPI. A confocal laser scanning microscope (FV1000; Olympus, Center Valley, PA) were used to image the coverslips.

Supplementary Figures and Figure Legends

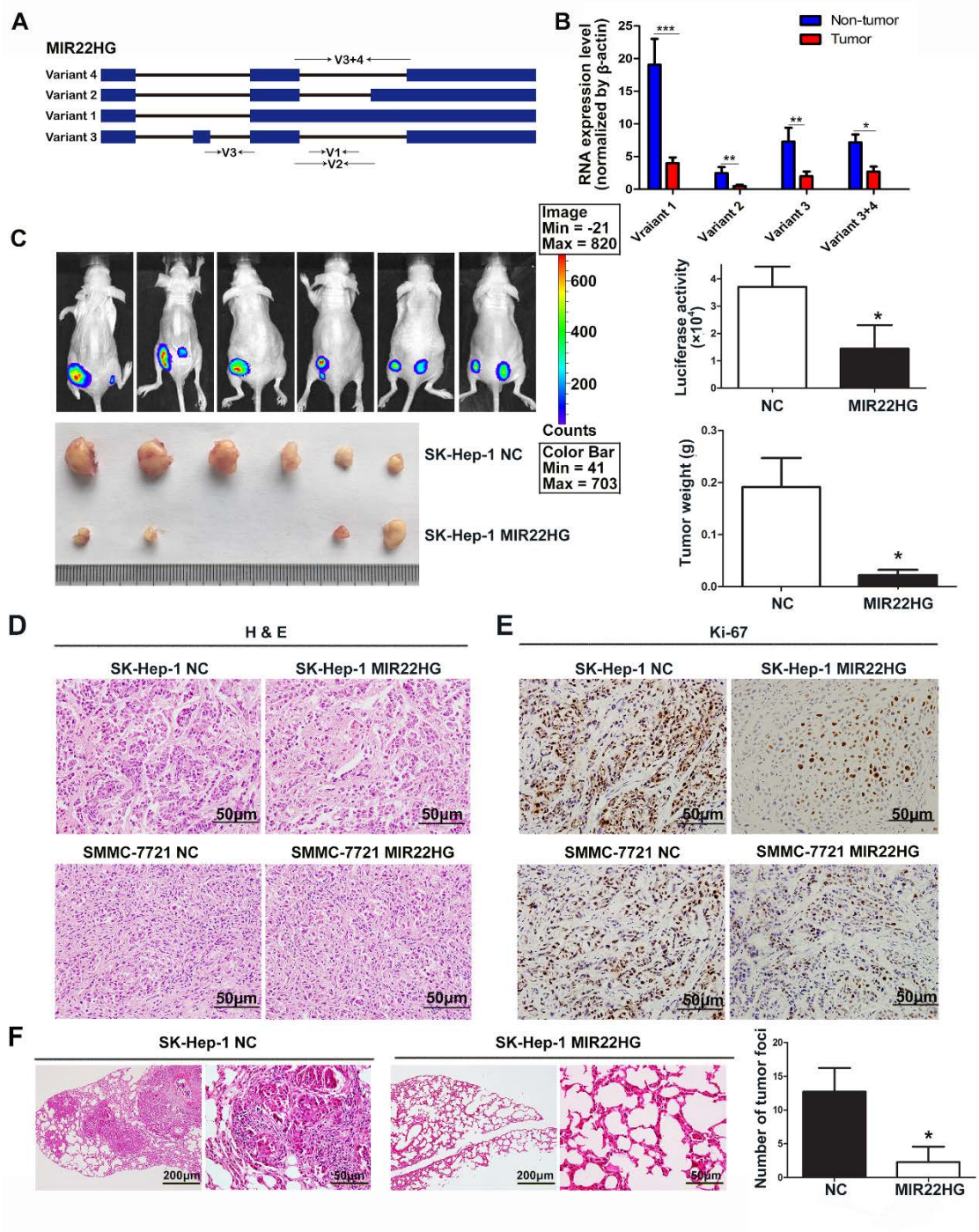

Supplementary Fig. 1. *MIR22HG* overexpression inhibits tumor growth and metastasis *in vivo*. (A) Schematic presentation of the *MIR22HG* transcripts. The primer pairs used to detect different variants of *MIR22HG* by RT-qPCR are indicated by arrows. (B) The expression levels of different variants of *MIR22HG* were detected

in 7 paired HCC tumor tissues and non-tumor tissues using RT-qPCR. Variant 1 was the most abundant isoform in non-tumor tissues but dramatically downregulated in tumor tissues, as its expression value peaked nearly 20 in non-tumor tissue but bottomed only 3.9 in tumor tissue. (C) *MIR22HG* overexpression in SK-Hep-1 cells inhibited tumor growth *in vivo*. The volume and weight of subcutaneous xenograft tumors were significantly different between the *MIR22HG* and control groups (n = 6). **P*< 0.05. (D) H&E-stained sections of xenograft tumors from the *MIR22HG* and control groups. (E) IHC staining for Ki-67 of xenograft tumors from the *MIR22HG* and control groups. (F) Representative microscopic images of H&E-stained pulmonary metastasis in the *MIR22HG*-overexpressing and control groups. Lung metastasis in both groups were quantified.**P*< 0.05.

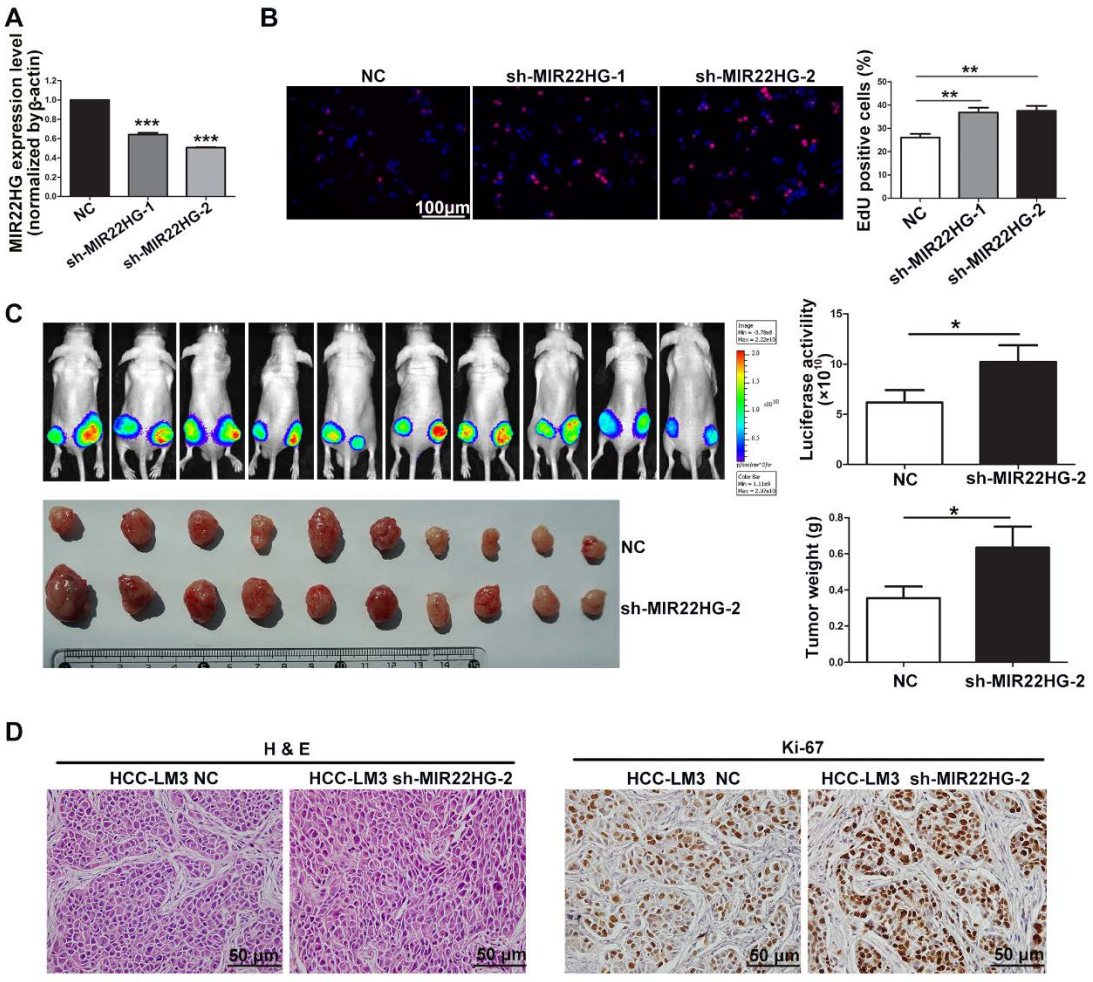

Supplementary Fig. 2. Knockdown of *MIR22HG* promotes tumor growth both *in vitro* and *in vivo*. (A) Knockdown efficiency of 2 different shRNAs specific to *MIR22HG* was examined in HCC-LM3 cells by qRT-PCR, ****P*< 0.0001. (B) *MIR22HG* deletion in HCC-LM3 cells promoted cellular proliferative capacity, ***P*< 0.01. (C) *MIR22HG* deletion in HCC-LM3 cells promoted tumor growth *in vivo*. HCC-LM3 cells with sh-*MIR22HG* (right side) and control vector (left side) were injected into the bilateral flanks of the nude mice. The volume and weight of subcutaneous xenograft tumors were significantly different between the sh-*MIR22HG* and control groups (n = 10). **P* < 0.05. (D) Left panel: H&E-stained sections of xenograft tumors from sh-*MIR22HG* and control groups. Right panel: IHC staining

for Ki-67 of xenograft tumors from the sh-*MIR22HG* and control groups.

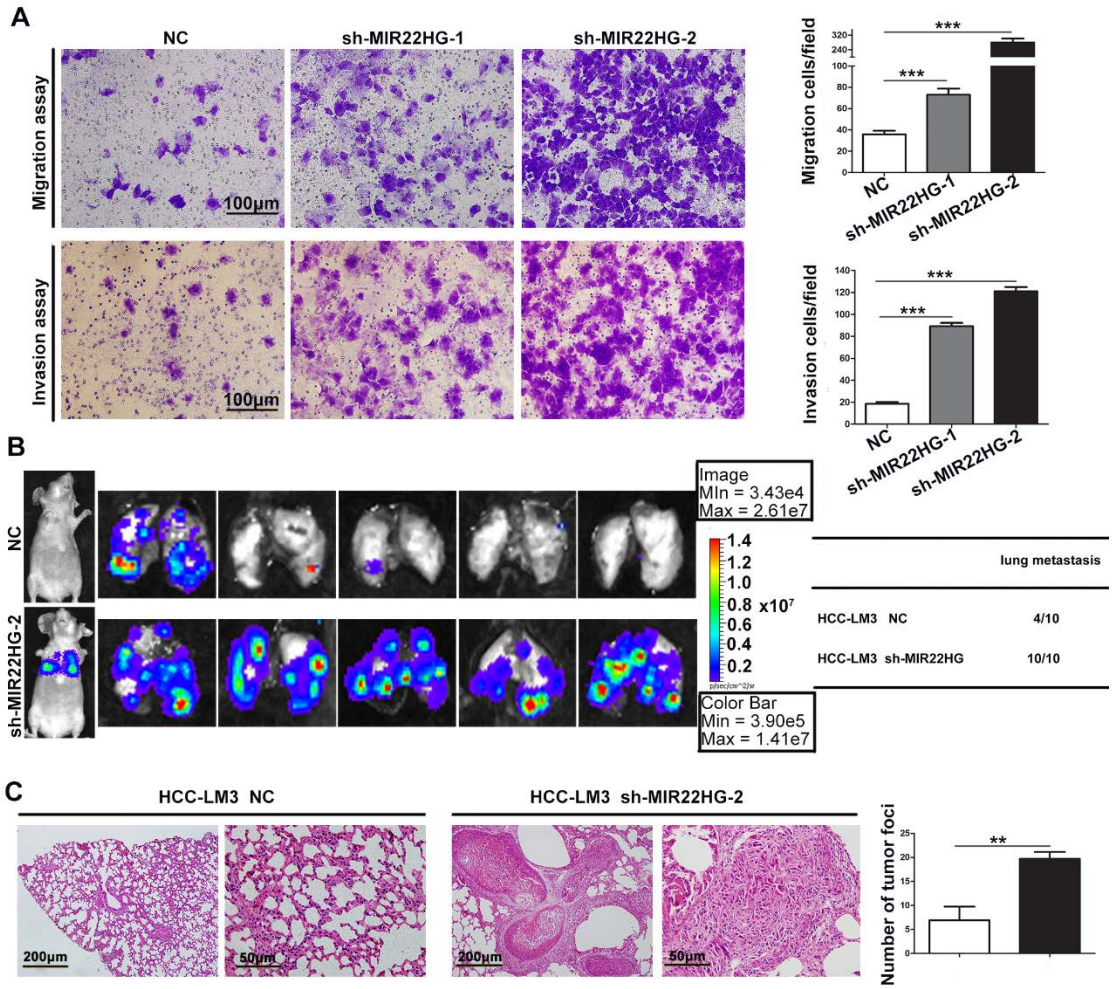

Supplementary Fig. 3. Knock down of *MIR22HG* promotes tumor invasion and metastasis both *in vitro* and *in vivo*. (A) Motility and invasive ability of HCC-LM3 cells after transfection of 2 different shRNAs specific to *MIR22HG* were evaluated by *in vitro* transwell assays. (B) sh-*MIR22HG*HCC-LM3 cells and control cells were injected intravenously into mice and bioluminescence images were obtained (n = 10). Left panel: Representative images of pulmonary colonization at 3 weeks after injection. Right panel: Numbers of mice with lung metastasis in both groups. (C) Representative microscopic images of H&E-stained pulmonary metastasis in the sh-*MIR22HG* and control groups. Lung metastasis in both groups were quantified.

* *P < 0.01.

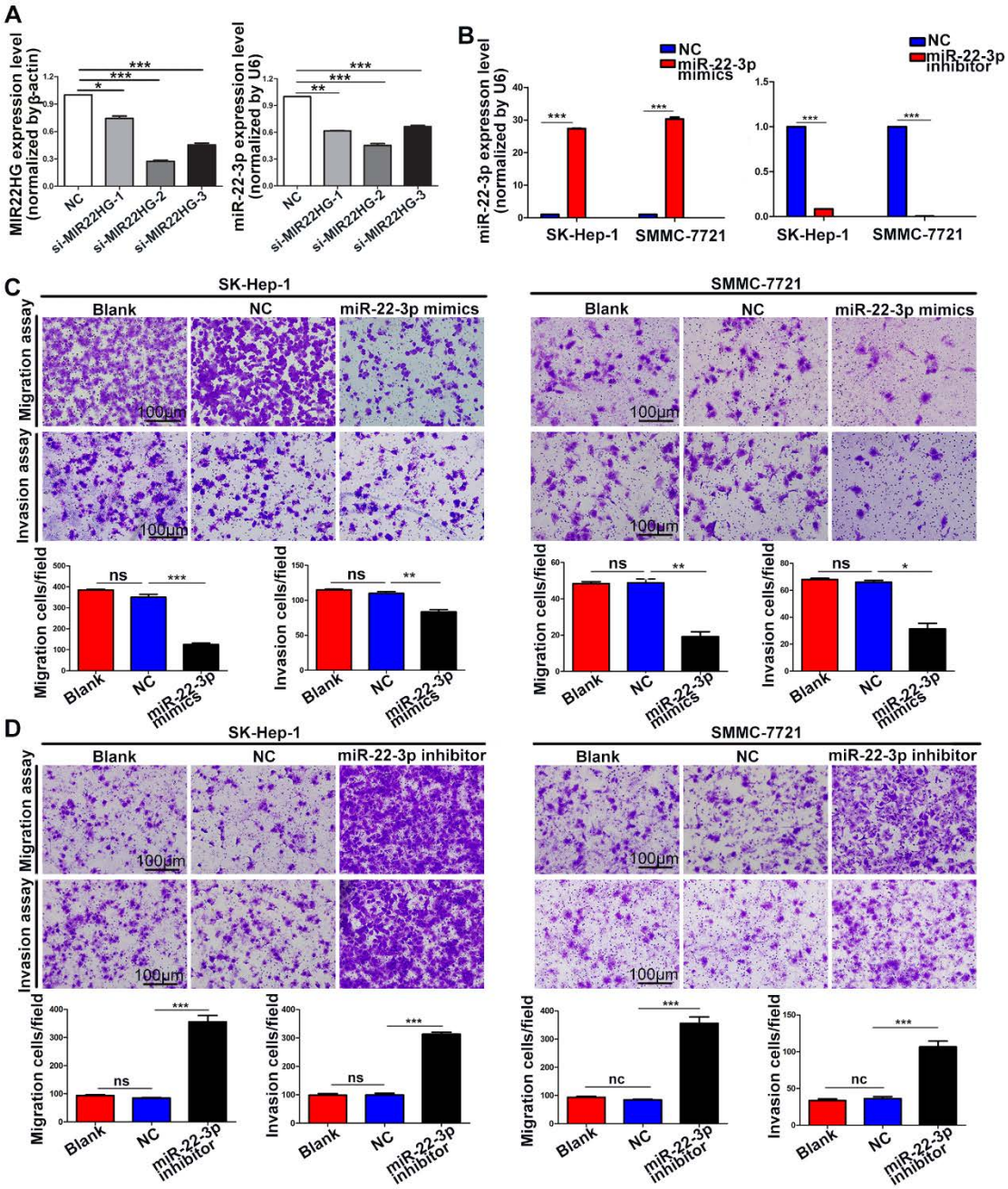

Supplementary Fig. 4. miR-22-3p inhibits cell migration and invasion. (A) miR-22-3p expression was detected in *MIR22HG* knockdown HCC-LM3 cells. *P< 0.05; **P < 0.01; ***P< 0.0001. (B) Expression of miR-22-3p was examined in SK-Hep-1 and SMMC-7721 cells transfected with miR-22-3p mimics (left panel) or miR-22-3p inhibitor (right panel). (C) Effects of miR-22-3p overexpression on

migration and invasion were detected in SK-Hep-1 and SMMC-7721 cells. (D) Effects of miR-22-3p inhibition on migration and invasion were detected in SK-Hep-1 and SMMC-7721 cells.

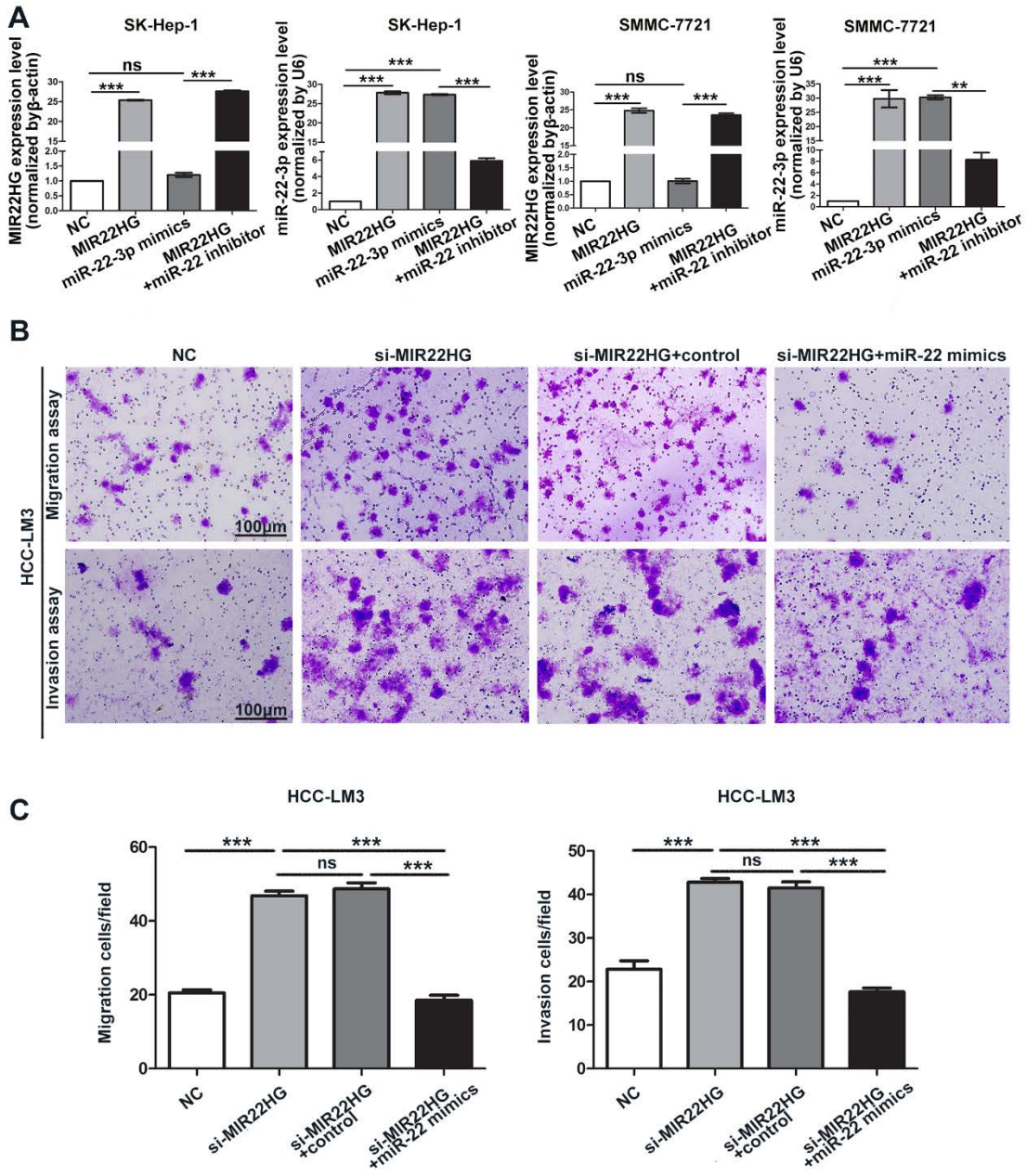

Supplementary Fig. 5. Up-regulation of miR-22-3p suppresses the promotion of migration and invasion by *MIR22HG* knockdown in HCC-LM3 cells. (A) Expression of *MIR22HG* and miR-22-3p were detected in the indicated conditions. ***P*< 0.01, ****P*< 0.0001, ns: not significant. (B) Representative images of migration

and invasion assays of the indicated cell lines. Silencing of *MIR22HG* promoted migration and invasion in HCC-LM3 cells, and these effects were destroyed by miR-22-3p mimics. (C) Quantification of cell migration and invasion in the indicated cell lines. Each bar represents the mean ± SEM of three independent experiments. ***P< 0.0001, ns: not significant.

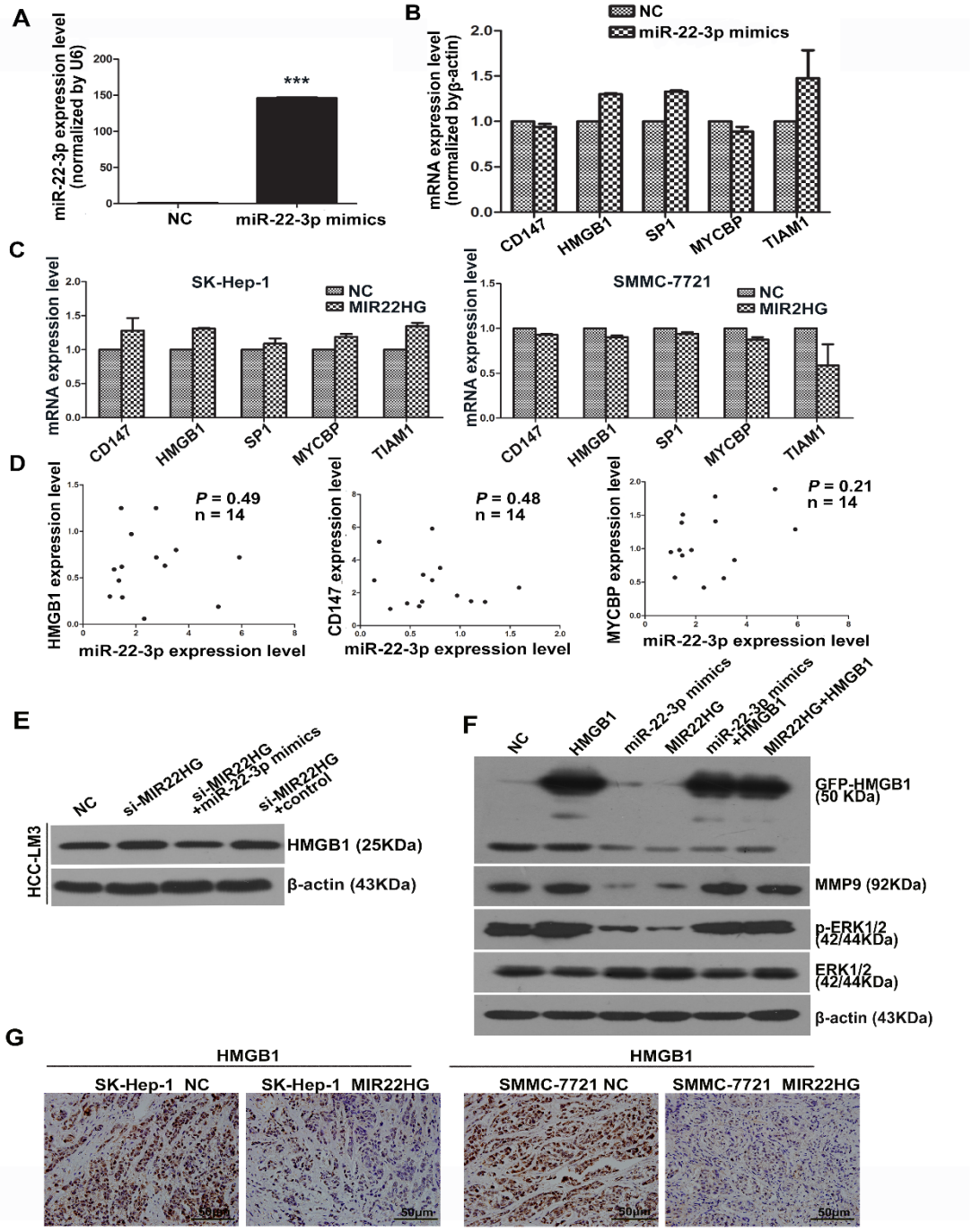

Supplementary Fig. 6. HMGB1 is regulated by *MIR22HG* in HCC. (A) miR-22-3p expression in SK-Hep-1 cells after transfection with miR-22-3p mimics. (B) mRNA expression of the indicted genes in SK-Hep-1 cells after transfection with miR-22-3p mimics. The mRNA expression of CD147, HMGB1, SP1, MYCBP, and TIAM1 did not alter after overexpression of miR-22-3p. (C) mRNA expression of the indicated genes in SK-Hep-1 and SMMC-7721 cells after transfection with *MIR22HG*. The mRNA expression of the indicated genes remained stable in spite of *MIR22HG* overexpression both in SK-Hep-1 and SMMC-7721 cells. (D) Correlation between miR-22-3p expression and mRNA expression of the indicated genes in 14 HCC tissues. The mRNA expression of the indicated genes did not correlate with miR-22-3p in 14 HCC tissues as measured by qRT-PCR. (E) Protein expression levels of HMGB1 in the indicated cell lines as determined by western blotting. The promotion effect of si-*MIR22HG* on HMGB1 expression was abolished by miR-22-3p mimics. (F) Expression of HMGB1 and its downstream effectors in SK-Hep-1 cell line as determined by western blotting. (G) HMGB1 expression in xenograft tumors developed by injecting indicated cells into nude mice as detected by IHC. The expression of HMGB1 was down-regulated in *MIR22HG*-overexpressing xenograft tumors.

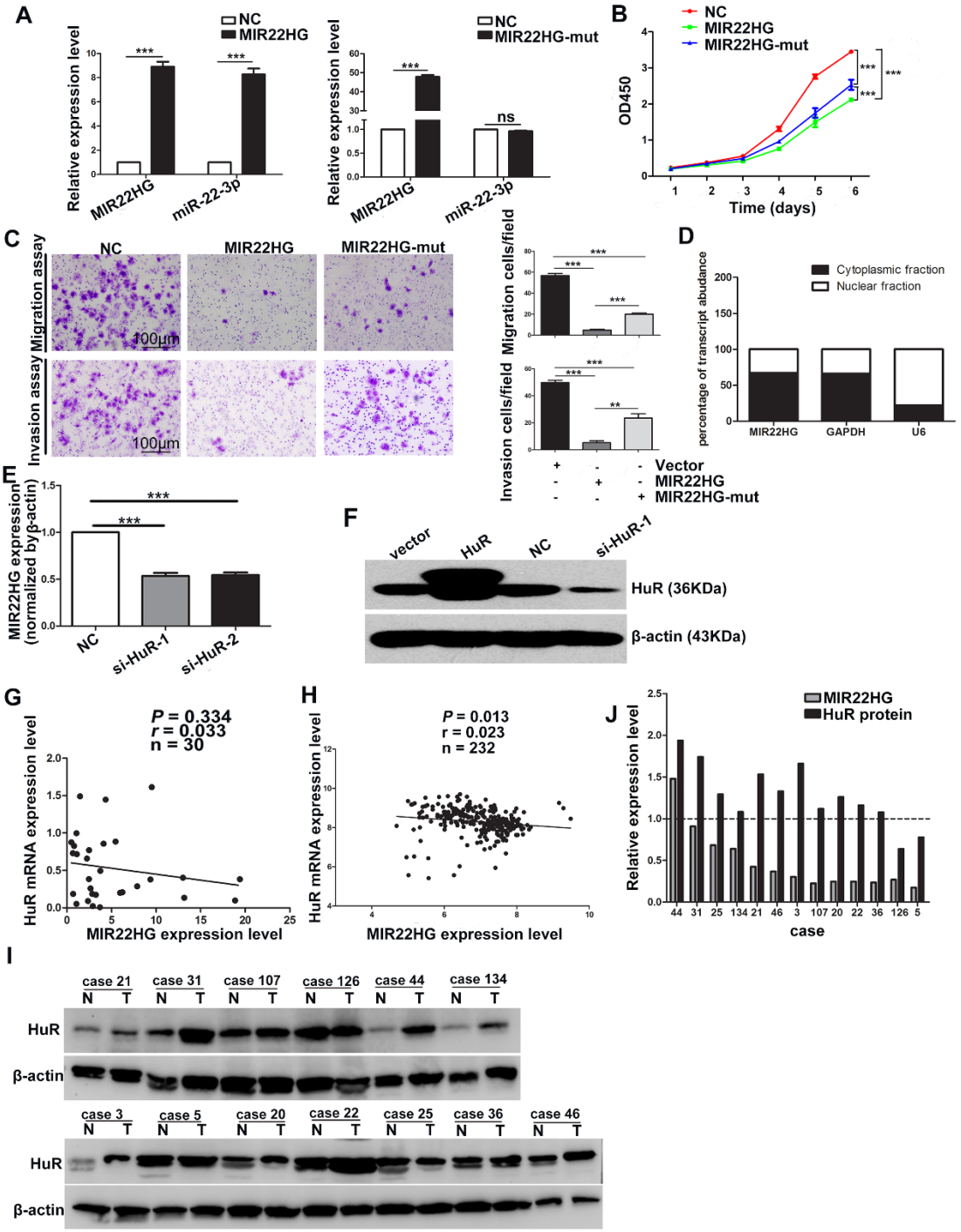

Supplementary Fig. 7. *MIR22HG*-mut inhibits cellular proliferation, migration, invasion of HCC cells. (A) Ectopic expression of *MIR22HG* induced miR-22-3p expression, whereas, ectopic expression of *MIR22HG* with miR-22-3p region deletion mutation (*MIR22HG*-mut) did not influenced the expression of miR-22-3p. ***P <

0.0001, ns: not significant**.** (B) Overexpression of *MIR22HG* and *MIR22HG*-mut significantly inhibited cellular proliferation as detected by CCK-8 assay. ***P < 0.0001. (C) *In vitro* migration and invasion assay showed that both *MIR22HG* and *MIR22HG*-mut repressed HCC cell migration and invasion. **P < 0.01, ***P < 0.0001. (D) Fractionation of SMMC-7721 cells followed by qRT-PCR indicated that *MIR22HG* mainly localized in cytoplasm. *U6* RNA served as a positive control for nuclear gene expression, and GAPDH RNA served as a positive control for cytoplasm gene expression. (E) The expression level of *MIR22HG* was examined in SMMC-7721 cells after transfection with HuR specific siRNAs. ***P < 0.0001. (F) Efficiency of HuR overexpression or silencing was evaluated by western blotting. (G-H) Correlation between HuR mRNA expression and *MIR22HG* expression level was detected in HCC tissues from 52-patient cohort (G) and GSE14520 (H), respectively. (I) HuR protein expression level was detected in 13 paired HCC tissues and non-tumor tissues from 52-patient cohort. (J) Correlation between HuR protein expression and *MIR22HG* expression level was analyzed.

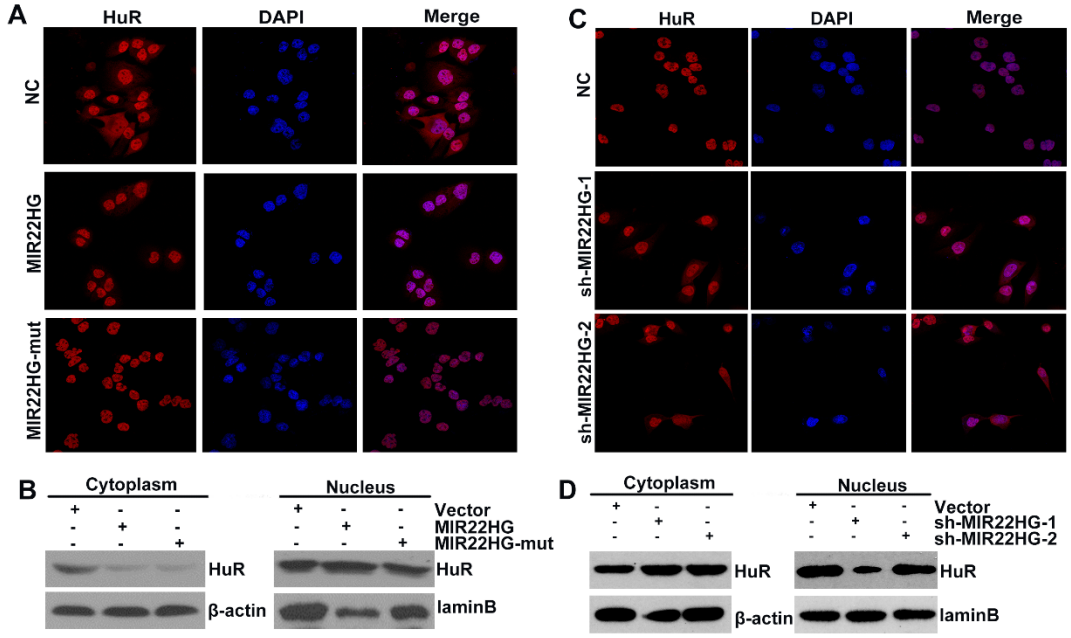

Supplementary Fig. 8. *MIR22HG* or *MIR22HG*-mut overexpression alters the subcellular localization of HuR.

(A) The translocation of HuR from the cytoplasm to the nucleus was detected by immunofluorescence staining after *MIR22HG* or *MIR22HG*-mut overexpression in SMMC-7721 cells. (B) Western blotting showed that HuR translocated from cytoplasm to the nucleus after *MIR22HG* or *MIR22HG*-mut overexpression in SMMC-7721. (C) The translocation of HuR from the nucleus to the cytoplasm was detected by immunofluorescence staining after *MIR22HG* deletion in HCC-LM3 cells. (D) Western blotting showed that HuR translocated from the nucleus to the cytoplasm after silencing *MIR22HG* in HCC-LM3 cells.

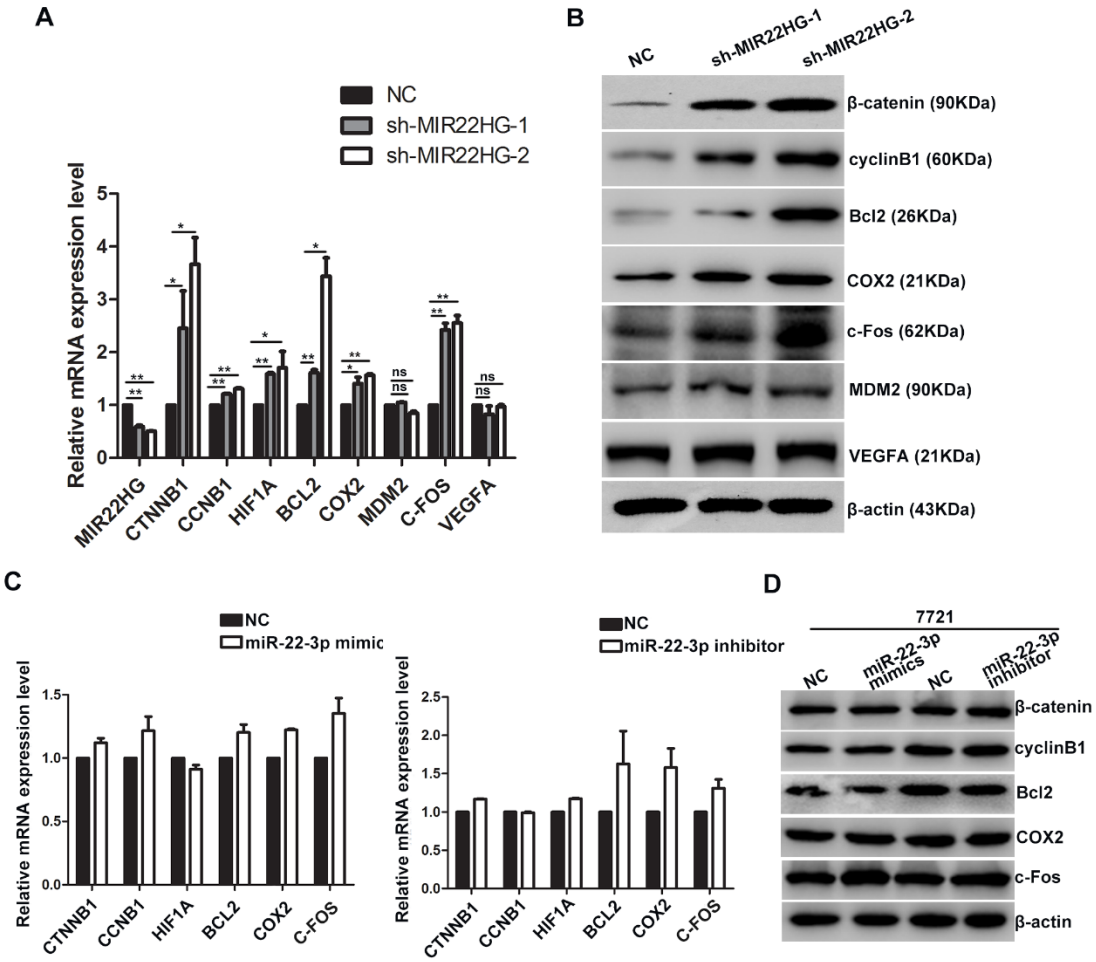

Supplementary Fig. 9. Silencing *MIR22HG* increases expression of the target genes of HuR. (A) Effect of *MIR22HG* knockdown on the mRNA expression of the indicated genes. (B) *MIR22HG* knockdown increased the expression of the indicated proteins. (C-D) The mRNA (C) and protein (D) expression of the indicated genes was detected in SMMC-7721 cells transfected with an miR-22-3p mimic and inhibitor.

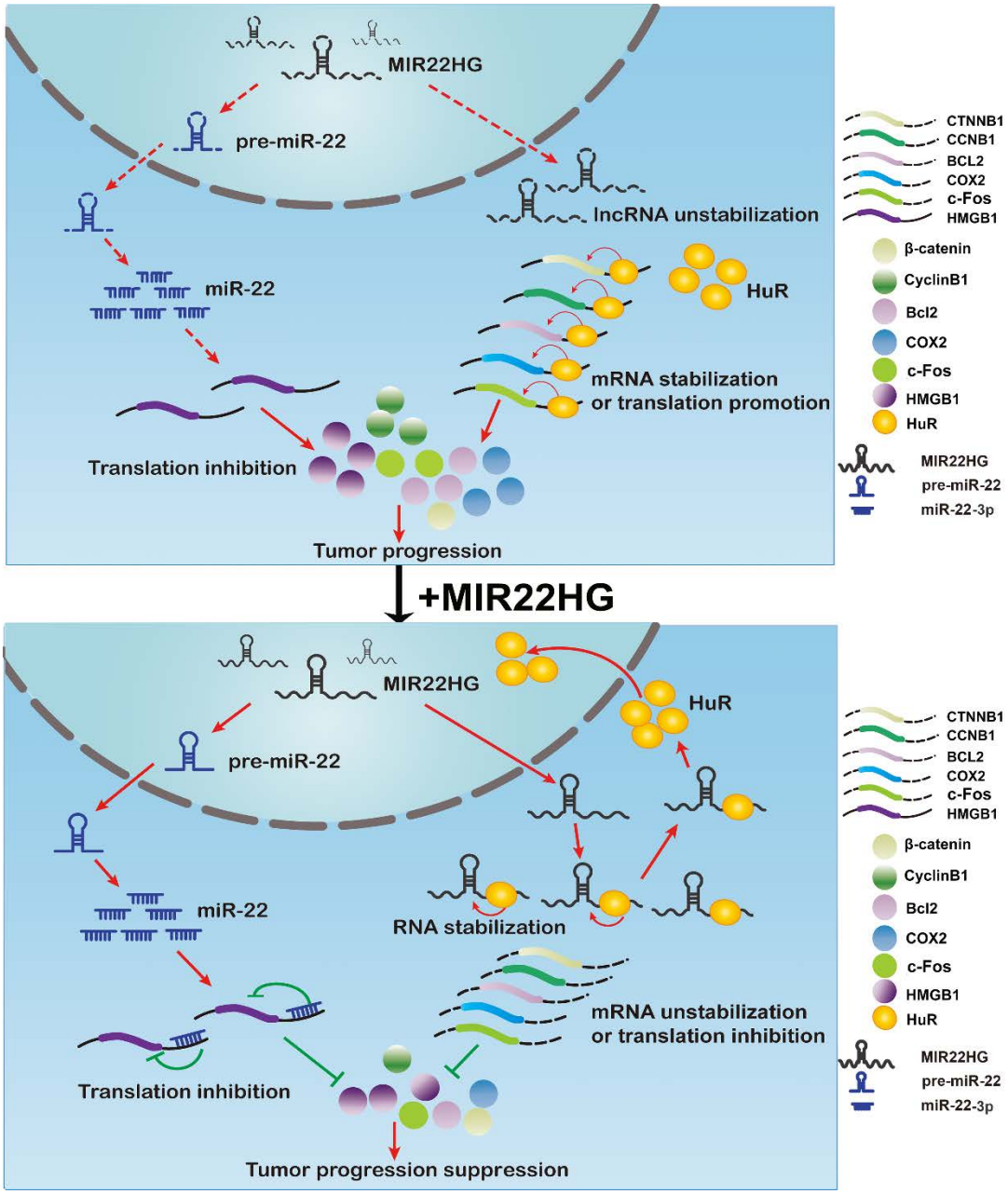

Supplementary Fig. 10. *MIR22HG* induces miR-22-3p to restrain HMGB1 translation and interacts with HuR, thus interrupting HuR binding to its target mRNAs.

In HCC cells, at the absence of *MIR22HG*, cytoplasmic HuR is able to stabilize or promote the translation of its target mRNAs including *CTNNB1*, *CCNB1*, *BCL2*, *COX2*，and *C-FOS*. The upregulation of these oncogenes results in tumor progression. Low level of *MIR22HG* also undergoes unstabilization due to its insufficient

interaction with HuR. When *MIR22HG* increases, it acts as a tumor suppressor in two aspects. Firstly, it generates pre-miR-22, the precursor for miR-22-3p which inhibits mRNA HMGB1 translation. Secondly, lncRNA *MIR22HG* competitively binds to HuR in cytoplasm, leading to the stabilization of *MIR22HG* and promoting the nuclear translocation of HuR; therefore, the expressions of the aforementioned HuR target mRNAs are restrained by *MIR22HG*-HuR interaction. In all, the presence of *MIR22HG* reduces the level of *CTNNB1*, *CCNB1*, *BCL2*, *COX2*, *C-FOS* and *HMGB1*, and hence restricts HCC progression.

Supplementary Tables

Supplementary Table 1

Clinicopathological characteristics of 52 HCC patients (52-patient cohort)

Feature	N（%）
Age(years)	
≤55	36 (69.2)
>55	16 (30.8)
Gender	
Male	45 (86.5)
Female	7 (13.5)
Tumour size (cm)	
≤5	22 (42.3)
>5	30 (57.7)
Edmondson Grade	
I-II	13 (25.0)
III-IV	39 (75.0)
BCLC stage	
A	30 (57.7)
B+C+D	22 (42.3)
Liver cirrhosis	
Yes	38 (73.1)
No	14 (26.9)
Portal vein tumour thrombus	

Yes	15 (28.8)
No	37 (71.2)
No. tumour	
Solitary	42 (80.8)
Multiple	10 (19.2)
HBV	
With	47 (90.4)
Without	5 (9.6)

Supplementary Table S2

Clinicopathological characteristics of 145 HCC patients (145-patient cohort)

Feature	N（%）
Age(years)	
≤55	76 (52.4)
>55	69 (47.6)
Gender	
Male	121 (83.4)
Female	24 (16.6)
Tumour size (cm)	
≤5	65 (44.8)
>5	80 (55.2)
Edmondson grade	
I-II	118 (81.4)
III-IV	27 (18.6)
BCLC stage	
A	103 (71.0)
B+C+D	42 (29.0)
Portal vein tumour thrombus	
No	125 (86.2)
Yes	20 (13.8)
Liver cirrhosis	
Yes	107 (73.8)
No	38 (26.2)
Metastasis	
Yes	6 (4.1)
No	139 (95.9)
Relapse	
Yes	48 (33.1)
No	97 (66.9)
No. tumour	
Solitary	116（80.0）
Multiple	29（20.0）
HBV	
With	124 (85.5)
Without	21 (14.5)

Supplementary Table 3

Correlation between *MIR22HG* expression and HCC clinicopathologic features in 145-patient cohort

	MIR22HG expression levels		*P*
	high expression	low expression	
Gender			0.939
Male	48	73	
Female	9	15	
Age (years)			0.535
≤55	22	54	
>55	35	34	
Edmondson Grade			**0.004***
I-II	53	65	
III-IV	5	22	
Liver cirrhosis			0.981
With	42	65	
without	15	23	
HBV			0.279
With	51	73	
Without	6	15	
Portal vein tumour thrombus			**0.004***
No	55	70	
Yes	2	18	
No. tumour			0.062
Solitary	50	66	
Multiple	7	22	
Tumour size (cm)			0.241
≤5	29	36	
>5	28	52	
BCLC stage			**0.005***
A	48	55	
B+C+D	9	33	
Relapse			0.164
Yes	15	33	
No	42	55	
Metastasis			0.587
Yes	3	3	
No	54	85	

Abbreviations: AFP, alpha-fetoprotein; BCLC, Barcelona Clinic Liver Cancer. *The values had statistically significant differences.

Supplementary Table S4

Overlapping genes predicted by miRanda and picTar

miRNA	GeneName
has-miR-22-3p	JARID2
has-miR-22-3p	PTPN1
has-miR-22-3p	CTSC
has-miR-22-3p	COPS7B
has-miR-22-3p	ELOVL6
has-miR-22-3p	IKZF4
has-miR-22-3p	GALNT3
has-miR-22-3p	SEMA6D
has-miR-22-3p	SIRT1
has-miR-22-3p	BIN1
has-miR-22-3p	CDKN1A
has-miR-22-3p	PIP4K2B
has-miR-22-3p	EDC3
has-miR-22-3p	SMG7
has-miR-22-3p	CALM3
has-miR-22-3p	STYX
has-miR-22-3p	CAMK2N1
has-miR-22-3p	MXD1
has-miR-22-3p	HOXA4
has-miR-22-3p	KDM3A
has-miR-22-3p	ZBTB39
has-miR-22-3p	PRPF38A
has-miR-22-3p	BCL9
has-miR-22-3p	EP300
has-miR-22-3p	PURB
has-miR-22-3p	FRAT2
has-miR-22-3p	IPO7
has-miR-22-3p	LRRC16A
has-miR-22-3p	NFYA
has-miR-22-3p	ERBB3
has-miR-22-3p	EMILIN3
has-miR-22-3p	TRUB1
has-miR-22-3p	FAM96A
has-miR-22-3p	BATF3
has-miR-22-3p	C15orf29

has-miR-22-3p	NCOA1
has-miR-22-3p	MAPK14
has-miR-22-3p	SRF
has-miR-22-3p	MYCBP
has-miR-22-3p	FBXO45
has-miR-22-3p	CD147
has-miR-22-3p	KDM6B
has-miR-22-3p	PHF8
has-miR-22-3p	ERGIC2
has-miR-22-3p	SV2A
has-miR-22-3p	NET1
has-miR-22-3p	DPF2
has-miR-22-3p	LRP12
has-miR-22-3p	BTBD10
has-miR-22-3p	WASF1
has-miR-22-3p	NR3C1
has-miR-22-3p	CTDSPL2
has-miR-22-3p	RTN3
has-miR-22-3p	UNK
has-miR-22-3p	SATB2
has-miR-22-3p	PPP1R15B
has-miR-22-3p	CCDC47
has-miR-22-3p	DPYSL3
has-miR-22-3p	STK39
has-miR-22-3p	FBXL19
has-miR-22-3p	MTF2
has-miR-22-3p	TIAM1
has-miR-22-3p	WRNIP1
has-miR-22-3p	BTG1
has-miR-22-3p	NRAS
has-miR-22-3p	SLC2A1
has-miR-22-3p	LRRC1
has-miR-22-3p	HERPUD2
has-miR-22-3p	FBXW7
has-miR-22-3p	LIN7C
has-miR-22-3p	ATXN7
has-miR-22-3p	UBE2K
has-miR-22-3p	HSPG2
has-miR-22-3p	CENPV
has-miR-22-3p	EPC1
has-miR-22-3p	LGALS1

has-miR-22-3p	STAG2
has-miR-22-3p	CYTH3
has-miR-22-3p	NAA20
has-miR-22-3p	DPY30
has-miR-22-3p	STX4
has-miR-22-3p	HMGB1
has-miR-22-3p	ITGB3BP
has-miR-22-3p	EFNA5
has-miR-22-3p	AKT3
has-miR-22-3p	MAT2A
has-miR-22-3p	CPEB1
has-miR-22-3p	GNB4
has-miR-22-3p	ZNRF2
has-miR-22-3p	CLDND1
has-miR-22-3p	RAB5B
has-miR-22-3p	HNRNPUL2
has-miR-22-3p	PDIK1L
has-miR-22-3p	MSL2
has-miR-22-3p	SP1
has-miR-22-3p	TCF7L2
has-miR-22-3p	PLCXD3
has-miR-22-3p	POGK
has-miR-22-3p	CHD7
has-miR-22-3p	DNM3
has-miR-22-3p	TP53INP1
has-miR-22-3p	FOXP1
has-miR-22-3p	C6orf62
has-miR-22-3p	NDEL1
has-miR-22-3p	MAX
has-miR-22-3p	SNRK
has-miR-22-3p	PLAGL2
has-miR-22-3p	FOSL1
has-miR-22-3p	RNF38
has-miR-22-3p	ETS2
has-miR-22-3p	FAM49B
has-miR-22-3p	RSBN1
has-miR-22-3p	TGFBR1
has-miR-22-3p	MACROD2
has-miR-22-3p	MAP2K4
has-miR-22-3p	C17orf58
has-miR-22-3p	ARFIP2

has-miR-22-3p	LAMC1
has-miR-22-3p	NUDT4
has-miR-22-3p	PTEN
has-miR-22-3p	MECOM
has-miR-22-3p	RFXANK

Supplementary Table S5

Primer sequence used in this study

Gene	sequence
MIR22HG (Variant1)-F	5′ ATCCAAAGCAGGACAGCA 3′
MIR22HG (Variant1)-R	5′ TGGCAGGTTTACACTCACT 3′
MIR22HG (Variant2)-F	5′ CCAGCTAAAGCTGCCAGTTG 3′
MIR22HG (Variant2)-R	5′ CAGACACAGCTTCCTTGGGT 3′
MIR22HG (Variant3)-F	5′ ACATTTCTGGACCTGAGGAGC 3′
MIR22HG (Variant3)-R	5′ GGGCAAAGGCTCTCCAACTT 3′
MIR22HG (Variant4)-F	5′ CGAACAGCAGGGTGGATGAT 3′
MIR22HG (Variant4)-R	5′ CGCACTATGGTGCCACATCT 3′
HMGB1-F	5′CGCTTTTGTGATGGAGTGCTG 3′
HMGB1-R	5′AAGGGAAAAACTTTGCCATCCCT 3′
MYCBP-F	5′CCATTACAAAGCCGCCGACTC 3′
MYCBP-R	5′CACTGTTAGGTTTCTCTGGTTCTTC 3′
SP1-F	5′ AATTTGCCTGCCCTGAGTGC 3′
SP1-R	5′ TTGGACCCATGCTACCTTGC 3′
CD147-F	5′ TCGCGCTGCTGGGCACC 3′
CD147-R	5′ TGGCGCTGTCATTCAAGGA 3′
TIAM1-F	5′ GCATTCCTGTGA CTGAGCAG 3′
TIAM1-R	5′ TCAGGAAGCCAATTCTCACG 3′
CTNNB1-F	5’ACAGGGAAGACATCACTGAGCC 3’
CTNNB1-R	5’CAGTGGGATGGTGGGTGTAAGA 3’
CCNB1-F	5’ GCACTTCCTTCGGAGAGCAT 3’
CCNB1-R	5’ TGTAGAGTTGGTGTCCATTCAC3’

BCL2-F	5’ GAACTGGGGGAGGATTGTGG 3’
BCL2-R	5’ ACAAAGGCATCCCAGCCTC3’
HIF1A-F	5’ TCTGGATGCTGGTGATTTGG 3’
HIF1A-R	5’ GCACCAAGCAGGTCATAGGT 3’
COX2-F	5’ CCGGGTACAATCGCACTTAT 3’
COX2-R	5’ GGCGCTCAGCCATACAG 3’
MDM2-F	5’ CGAGCTTGGCTGCTTCT 3’
MDM2-R	5’ ACATTTGCCTGCTCCTCAC3’
VEGFA-F	5’ CGCAAGAAATCCCGGTATAA 3’
VEGFA-R	5’ TCTCCGCTCTGAGCAAGG 3’
C-FOS-F	5’ GGGGCAAGGTGGAACAGTTAT 3’
C-FOS-R	5’ AGGTTGGCAATCTCGGTCTG 3’
HuR-F	5’ AGAGATTCAGGTTCTCCCCCA 3’
HuR-R	5’ CCTGCCCCAGGTTGTAGATG 3’
miR-22-3p-RT	5′CTCAACTGGTGTCGTGGAGTCGGCAATTC AGTTGAGACAGTTCT 3′
miR-22-3p-F	5′ACACTCCAGCTGGGAAGCTGCCAGTTGA AG 3′
U6-F	5′CTCGCTTCGGCAGCACA 3′
U6-R	5′ AACGCTTCACGAATTTGCGT 3′
psiCHECK-HMGB1 -wt-F	5′CCGCTCGAGCGAGCCACTAACCTTGCCTG GTACA3′
psiCHECK-HMGB1 -wt-R	5’ATAAGAATGCGGCCGCTAAACTATGACA AAAGCTTTTTATTAGC 3′

Supplementary Table S6

Small-interfering RNA sequences used in this study

siRNA	sense sequence	anti-sense sequence
si-MIR22HG-1	5’ cccaagguuaguuggucuutt 3’	5’ aagaccaacuaaccuugggtt 3’
si-MIR22HG-2	5’ gcccagccuguaauguuuatt 3’	5’ uaaacauuacaggcugggctt 3’
si-MIR22HG-3	5’ ggcuuccuggaugacaguutt 3’	5’ aacugucauccaggaagccttt 3’

Supplementary Table S7

Information on antibodies used in this study

Antibody	WB	IHC	IF	Specificity	Company
HMGB1 (ab79823)	1: 1000	1:200	/	Mouse monoclonal	Abcam
CD147 (BS6536)	1:1000	/	/	Rabbit polyclonal	Bioworld Technology
β-actin (sc-8432)	1:2000	/	/	Mouse monoclonal	Santa Cruz Biotechnology
TIAM1 (ab70225)	1:1000	/	/	Rabbit polyclonal	Abcam
SP1(BS3622)	1:1000	/	/	Rabbit polyclonal	Bioworld Technology
MYCBP (ab66331)	1:1000	/	/	Rabbit polyclonal	Abcam
MMP9 (sc-10737)	1:1000	/	/	Rabbit polyclonal	Santa Cruz Biotechnology
ERK1/2 (#9102)	1:1000	/	/	Rabbit polyclonal	Cell Signaling Technology
p-ERK1/2 (#4370)	1:1000	/	/	Rabbit polyclonal	Cell Signaling Technology
Ki-67 (BS1454)	/	1:100	/	Rabbit polyclonal	Bioworld Technology
HuR (SC5261)	1:1000	/	1:100	Mouse monoclonal	Santa Cruz Biotechnology
β-catenin (ab32572)	1:1000	/	/	Rabbit polyclonal	Abcam
CyclinB1 (BS1392)	1:1000	/	/	Rabbit polyclonal	Bioworld Technology
Bcl2 (1017-1)	1:1000	/	/	Rabbit polyclonal	EPITOMICS
COX2 (sc-514489)	1:1000	/	/	Mouse monoclonal	Santa Cruz Biotechnology
c-Fos (sc-413)	1:1000	/	/	Mouse monoclonal	Santa Cruz Biotechnology
MDM2 (S160)	1:1000	/	/	Rabbit polyclonal	Bioworld Technology
VEGFA (sc-507)	1:1000	/	/	Rabbit polyclonal	Santa Cruz Biotechnology